energies

*Article*

# Mechanical Stress in Rotors of Permanent Magnet Machines—Comparison of Different Determination Methods

**Christian Monissen [1], Mehmet Emin Arslan [1], Andreas Krings [2] and Jakob Andert [1,*]**

[1] Teaching and Research Area Mechatronics in Mobile Propulsion, Faculty of Mechanical Engineering, RWTH Aachen University, Forckenbeckstraße 4, 52074 Aachen, Germany
[2] FEV Europe GmbH, Neuenhofstr. 181, 52048 Aachen, Germany
* Correspondence: andert@mmp.rwth-aachen.de

**Abstract:** In this work, different analytical methods for calculating the mechanical stresses in the rotors of permanent magnet machines are presented. The focus is on interior permanent magnet machines. First, an overview of eight different methods from the literature is given. Specific differences are pointed out, and a brief summary of the analytical approach for each method is provided. For reference purposes, a finite element model is created and simulated for each rotor geometry studied. A total of seven rotors rom representative automotive powertrains are considered in their specific speed range. The analytical methods are used to determine the maximum mechanical stress concentration factors for the seven rotor geometries, in which we are determined to find maximum mechanical stress as a final step of the analytical process. For each geometry and each respective operating speed range, the deviations from the finite element reference are determined. In addition, the error in the selected geometry variations is evaluated. A recommendation for the method with the lowest error considering all cases studied is given specifically for the stress in the airgap bridge and the central bridge.

**Keywords:** maximum mechanical stress; interior permanent magnet synchronous machine; finite element analysis; high-speed e-machine; stress concentration factor; analytical methods

check for updates

**Citation:** Monissen, C.; Arslan, M.E.; Krings, A.; Andert, J. Mechanical Stress in Rotors of Permanent Magnet Machines—Comparison of Different Determination Methods. *Energies* **2022**, *15*, 9169. https://doi.org/10.3390/en15239169

Academic Editors: Kan Liu and Wei Hu

Received: 8 November 2022
Accepted: 30 November 2022
Published: 3 December 2022



## 1. Introduction

Mechanical stress analysis for rotor geometries is particularly important when considering the ongoing trend toward higher speeds in electric machines for traction applications. An overview of this is given in [1] for commercially available battery or hybrid electric vehicles.

The traction machines of the Toyota Prius across the generations can serve as an example. Here, it can be seen that with approximately the same rotor diameter range, the maximum speed has increased from 6000 rpm in the first Prius generation introduced in 1997 to 17,000 rpm in the fourth generation introduced in 2015 [2,3]. With increased speed and the same radial rotor dimensions, the resulting centrifugal forces increase accordingly. These centrifugal forces act on the rotor and cause high mechanical stresses in certain areas, depending on the rotor pole geometry [4,5].

The maximum mechanical stresses (MMS) in the rotor are limited by the yield strength of the materials. The commonly used electric steel materials have yield strength values between 320 and 500 MPa [6,7], and the electrical machines on the market for traction applications have MMS values mainly in that range. As an example, Figure 1 shows finite element analysis (FEA) results of the MMS of a rotor based on the electric machine of the Toyota Prius III at its maximum speed of 13,500 rpm.

The MMS estimation in a rotor configuration is typically carried out by static mechanical FEA [7–11]. However, the convergence of the solution strongly depends on the mesh size and quality. The time for re-meshing and solving after each iteration, as well as extra computational effort for MMS estimation, must be considered [12,13]. To reduce time and computational cost, several analytical methods using simplified equivalent models to determine the average mechanical stress in these rotors have been proposed in the literature.

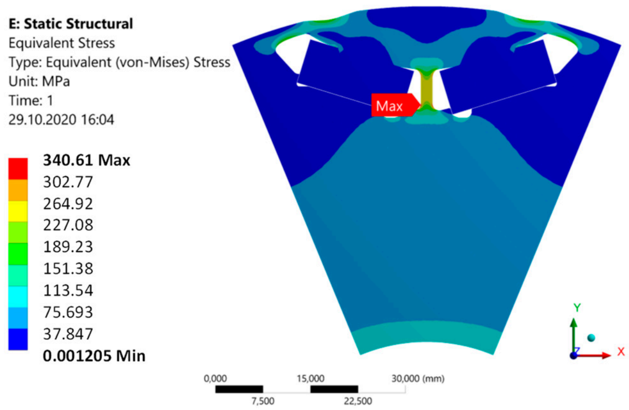


**Figure 1.** Distribution of von Mises stresses of Toyota Prius III rotor at 13,500 rpm.

To obtain a meaningful value for MMS based on average mechanical stress, a stress concentration factor (SCF) should be determined at the intersections where the geometric cross-section changes drastically [12–18]. Figure 2 shows a generic rotor pole of an interior permanent magnet synchronous machine (IPMSM). The areas where MMS mainly occurs are the intersection points of the air gap bridges and the central bridges (circled).

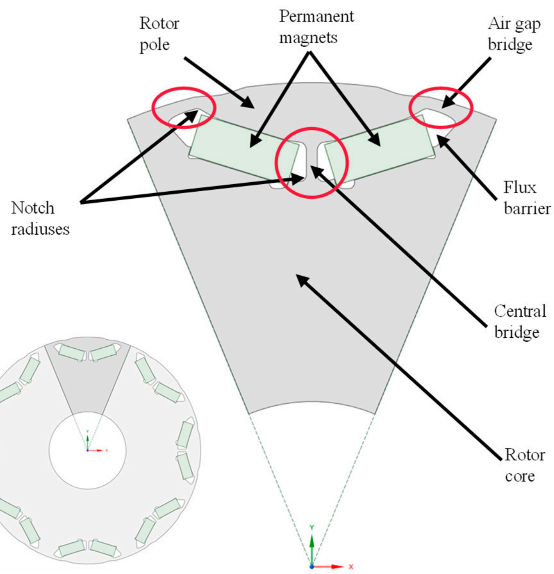


**Figure 2.** Definition of a single-pole rotor geometry definition marked areas where MMS can occur.

The approach of using equivalent mechanical models for the stress analysis in electrical machine rotor configurations is relatively new. Table 1 shows the methods studied with their publication date. The equivalent ring method (ERM), the centrifugal force method (CFM) and the beam theory method (BTM) are proposed to determine MMS on the air gap bridges using different approaches. The ERM method has evolved throughout the years with improvements and simplifications in the calculations. Therefore, there are five different ERM methods [12,13,15,19–21]. In this paper, the different ERM methods are chronologically referred to as ERM1 to ERM5. The central bridge method (CBM) and BTM method determine the MMS at the central bridges of V-shaped rotor geometries using different approaches [12,18,22].

**Table 1.** Analytical methods proposed in the literature for determining the maximum mechanical stress of an IPMSM.

| Analytical Methods | Year of Publication | Author | Applied on |
|---|---|---|---|
| ERM1 | 2002–2006 | Schätzer [19]–Binder et al. [20] | Air gap bridges |
| ERM2 | 2014 | Li Yi et al. [21] | Air gap bridges |
| ERM3 | 2016 | Chai et al. [12] | Air gap bridges |
| ERM4 | 2018 | Chu et al. [15] | Air gap bridges |
| ERM5 | 2020 | Chu et al. [13] | Air gap bridges |
| CFM | 2020 | Chu et al. [13] | Air gap bridges |
| BTM | 2018 | Kleilat et al. [18] | Air gap and central bridges |
| CBM | 2016 | Chai et al. [12] | Central bridges |

Chu et al. [15] proposed an SCF for the air gap bridges on flat rotor geometries by using the polynomial surface fitting technique. Chai et al. [12] and Bremner et al. [17] proposed two different references: Peterson's stress concentration [16] and Roark's formulas for stress and strain [23] to determine SCF at points where MMS occur.

The listed analytical methods have been developed recently and are validated in the literature only for basic rotor geometries. Consequently, the comparison of accuracy and stability of these proposed methods needs to be further investigated. The evaluation of the most accurate and stable analytical methods is performed by applying the methods to current geometries of IPMSM traction drives available on the market. The results are compared to detailed FEA simulations in Ansys® Mechanical, Release 18.1. The most suitable method can finally be included in the pre-design processes and can significantly reduce the computational effort.

## 2. Materials and Methods

### *2.1. Analytical Methods to Determine the Maximum Mechanical Stress at the Air Gap Bridge and the Central Bridge*

The process of each method and their main differences are shown in Figures 3 and 4.

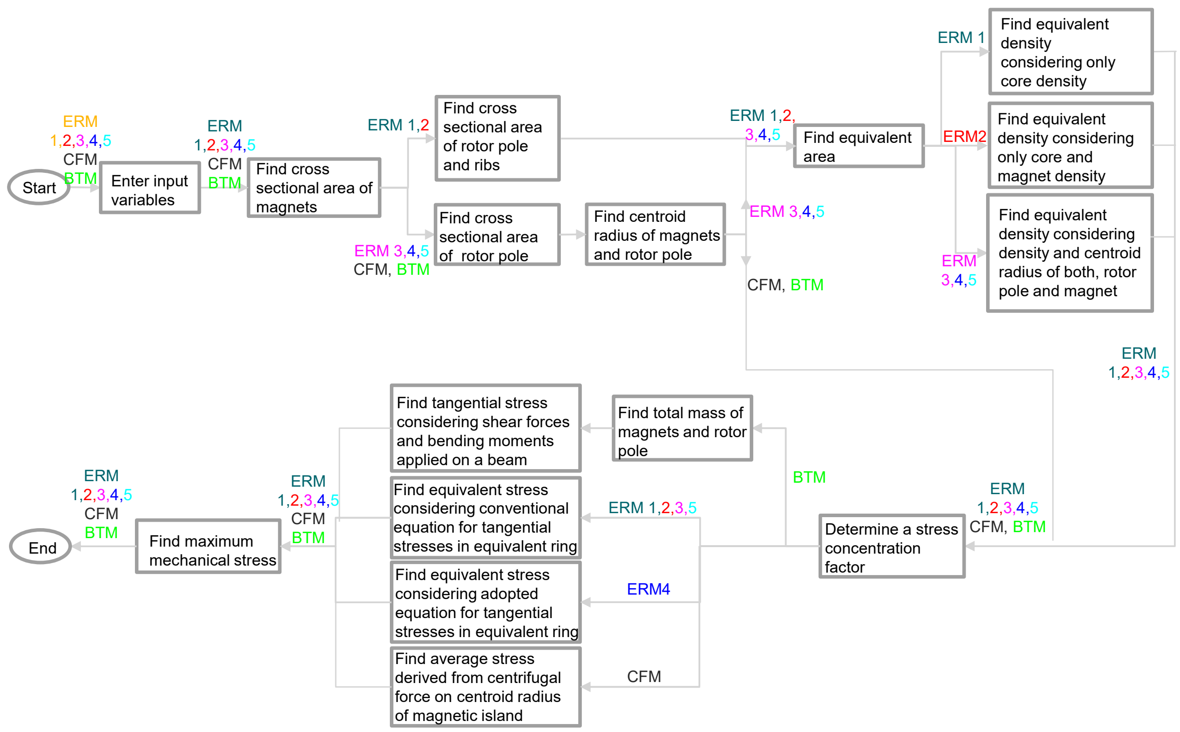


**Figure 3.** Methodology flow diagram of ERM1 to ERM5, CFM and BTM and general differences in the approaches.

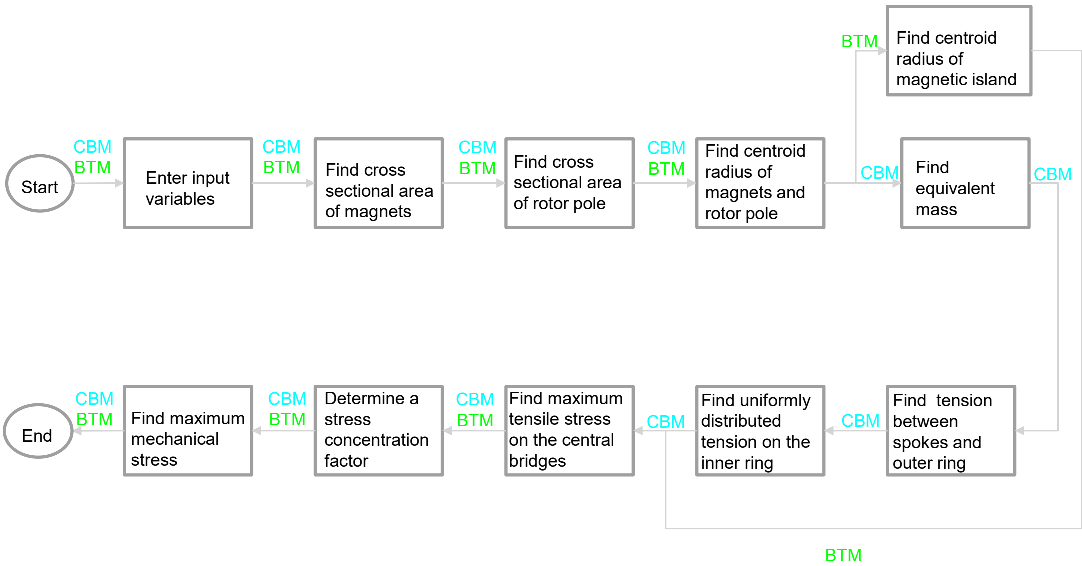


**Figure 4.** Methodology flow diagram of BTM and CBM and general differences in the approaches.

The most relevant parameters of an IPMSM are defined in Figure 5, the nomenclature of the regions is shown in Figure 1. The nomenclature and parameter definition for a V-shaped rotor geometry are analogous to the flat-shaped rotor geometries. $R_0$ is the outer radius of the rotor, d is the length of the airgap bridge, $r_a$ is the outer radius, $r_c$ is the inner radius of the magnet pocket, h is the magnet height, t is the length of central separation of magnet pockets, θ is the opening angle of the V-shape of the magnet, and α is the angle between the position of $r_a$ to the center of the magnet pole.

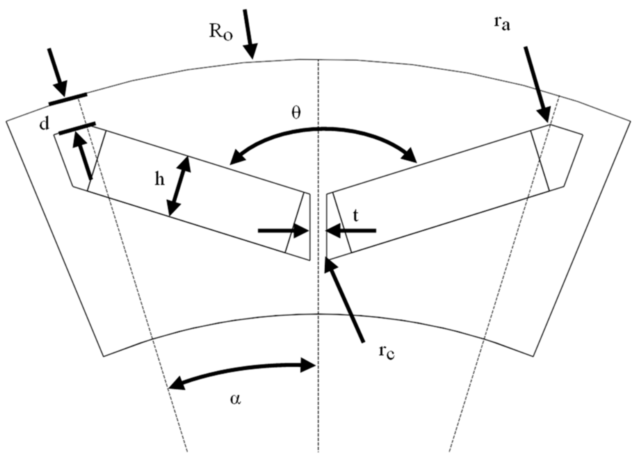


**Figure 5.** Parameter definition of a typical V-shaped rotor geometry (only the investigated parameters are shown).

Figure 6 shows the basic equivalent geometry approaches of each proposed method in the literature. In general, all methods define a simplified geometry, with an equivalent mass based on geometry and materials under investigation. In methods ERM2 to ERM5, the magnet-surrounding core material and the magnet are considered. For the ERM1 method only, the core material is considered. In ERM methods, only one ring is positioned at the airgap bridge representing the simplified geometry, as shown in Figure 6. With ERM1 and ERM2, no centroid radius of magnets and rotor poles are used, only the cross-sectional areas of rotor pole and ribs. With ERM3 to ERM5, these geometric quantities are considered, resulting in a more realistic representation of the model. All ERM methods use a sole ring at the outer radius of the rotor, which also limits the applicability of the stress estimation on the stress in the airgap bridge. This limitation must be considered when the maximal mechanical stress occurs in other regions of the rotor. Although a more detailed equivalent geometry is used in the CFM method, a similar limitation to the ERM method applies since no central bridge is represented. The stress in the central bridge can only be captured by the BTM and CBM methods mentioned above. Both methods also consider the central bridge by a beam or spoke, respectively, cf. Figure 6c,d. In the following, all mentioned methods are briefly recapitulated, and the equations of equivalent stress and maximum stress are given.

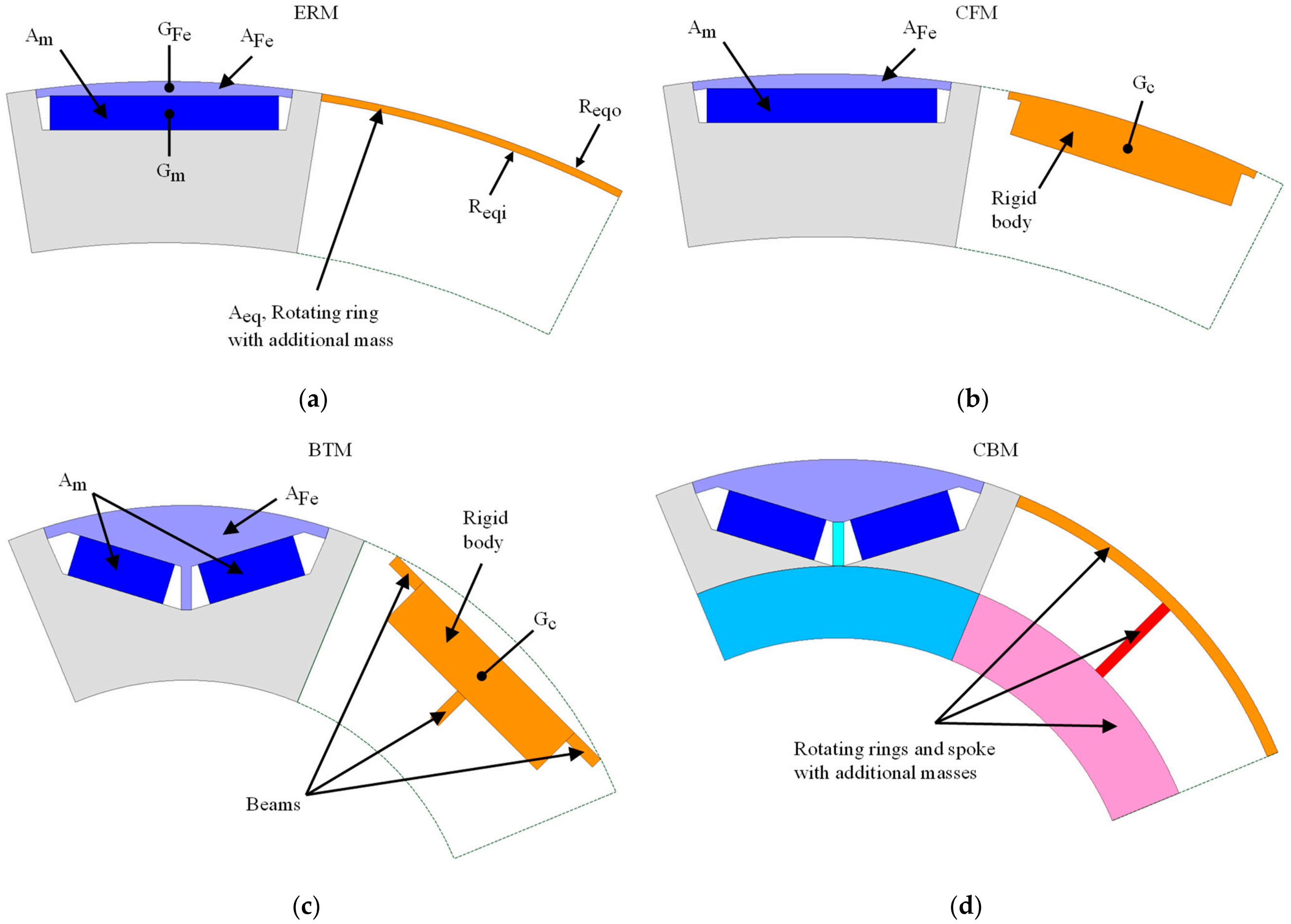


**Figure 6.** Real and equivalent models of analytical methods proposed in the literature: (**a**) ERM method, (**b**) CFM method, (**c**) BTM method, (**d**) CBM method.

First, the ERM1 method [19,20] is considered, which approximates the rotor pole and magnets as an equivalent ring model with additional mass density. The thickness of the ring is equal to the narrowest thickness of the air gap bridges. The authors introduced the equivalent density $\rho_{eq,erm1}$ as:

$$\rho_{eq,erm1} = \rho_{Fe} \cdot \frac{A_{Fe}+A_m}{A_{eq}}, \quad (1)$$

where $\rho_{Fe}$ is the mass density of electric steel in kg/m$^3$. $A_{Fe}$, $A_m$ and $A_{eq}$ represent the cross-sectional area of the rotor pole, the permanent magnets and the equivalent ring, respectively, as shown in Figure 6a. It can be observed that only the density of the electric steel is assumed for the whole considered region.

The tangential stresses $\sigma_{eq,erm1}$ and MMS $\sigma_{eq,max1}$ inside the equivalent ring are calculated as:

$$\sigma_{eq,erm1} = \left(\frac{R_{eqo}+R_{eqi}}{2}\right)^2 \cdot \omega^2 \cdot \rho_{eq,erm1}, \tag{2}$$

$$\sigma_{eq,max1} = k_{air\ gap\ bridge} \cdot \sigma_{eq,erm1}, \tag{3}$$

Here, $R_{eqo}$ and $R_{eqi}$ represent the outer and inner radius of the equivalent ring, respectively, as shown in Figure 6a. $\omega$ is the rotational speed in rad/s, and $k_{air\ gap\ bridge}$ is the SCF at the air gap bridges, which is introduced in Section 2.2 Determination of Stress Concentration Factors.

Equation (1) is improved in the ERM2 method [21] by also considering the mass density of magnets:

$$\rho_{eq,erm2} = \frac{\rho_{Fe}A_{Fe}+\rho_m A_m}{A_{eq}}, \tag{4}$$

where $\rho_m$ is the mass density of the magnet material.

ERM3 method uses Equation (4) and is further developed by taking the centroid radii of magnets and the rotor pole into account with:

$$\rho_{eq,erm3} = \frac{(R_{Fe}\rho_{Fe}A_{Fe}+R_m\rho_m A_m)\frac{1-\cos(\theta)}{2}}{R_0 A_{eq}}, \tag{5}$$

where $R_{Fe}$ and $R_m$ stand for the distance between the rotor center and the center of gravity of rotor pole $G_{Fe}$ and center of gravity of the permanent magnets $G_m$, respectively. $\rho_m$ is the mass density of the permanent magnet in kg/m$^3$. $\theta$ represents the angle between two magnets of a single pole in rad (see Figure 5). The centroid radius of the equivalent ring $R_0$ is calculated as:

$$R_0 = \left(\frac{R_{eqo}+R_{eqi}}{2}\right), \tag{6}$$

The calculations in Equation (5) are simplified in the ERM4 method [15], and Equation (2) is replaced by an adopted $\sigma_{eq,erm4}$ as:

$$\sigma_{eq,erm4} = \frac{\rho_{eq,erm4}\omega^2}{8}\left[(3+\nu)\left(R_{eqo}^2(1+R_{eqi})+R_{eqi}^2\right)-(1+3\nu)\,R_{eqi}^2\right], \tag{7}$$

where $\nu$ is the Poisson's ratio of electric steel, and $\rho_{eq,erm4}$ is the equival $\rho_{eq,erm4}$ is the equivalent density for the ERM4 method as:

$$\rho_{eq,erm4} = \frac{R_m\rho_m A_m + R_{Fe}\rho_{Fe}A_{Fe}}{R_0 A_{eq}}, \tag{8}$$

In the ERM5 method [14], the simplifications in the ERM4 method are used, but instead of using Equation (7) to determine the tangential stresses, the initial approach, Equation (2), is used again.

The CFM method considers rotor pole and magnets as a rigid body [13]. By performing a force analysis on that rigid body, average stresses at the air gap bridges $\sigma_{cfm}$ are determined as:

$$\sigma_{cfm} = \frac{(\rho_m A_m+\rho_{Fe}A_{Fe})\omega^2 R_c}{2\sin(\frac{\alpha}{2})d} \tag{9}$$

where $R_c$ is the distance between the rotor center and the center of gravity of magnets with rotor pole $G_c$ as shown in Figure 6b. d is the air gap bridge thickness and $\alpha$ is half pole arc in rad as shown in Figure 5.

The BTM method simplifies the air gap bridges and central bridges to simple rectangular beams and considers the rotor pole with magnets as a rigid body, as can be seen in

Figure 6c [18,22]. Average mechanical stresses at the air gap bridges $\sigma_{\text{btm,air gap bridge}}$ and central bridges $\sigma_{\text{btm,central bridge}}$ are given as:

$$\sigma_{\text{btm,air gap bridge}} = \left( \frac{\sqrt{c2^2 + \left(6 \cdot \frac{c3}{d}\right)^2} \omega^2}{l_{\text{stack}}} \right) \frac{m_{\text{total}} R_c}{d} \tag{10}$$

$$\sigma_{\text{btm,central bridge}} = \left( \frac{c1 \cdot \omega^2}{l_{\text{stack}}} \right) \frac{m_{\text{total}} R_c}{t} \tag{11}$$

where c1, c2 and c3 represent constant coefficients that quantify the relationship between centrifugal force, normal force and bending moment, respectively. The coefficients must be fitted to the FEA results. After the initial FEA calculation, these coefficients must be adjusted so that the FEA result matches the analytical result. $l_{\text{stack}}$ and t are the stack length and the central bridge thickness, respectively. The total mass of the rotor pole with magnets $m_{\text{total}}$ is expressed as:

$$m_{\text{total}} = (\rho_{\text{Fe}} A_{\text{Fe}} + \rho_m A_m) \cdot l_{\text{stack}} \tag{12}$$

In the CBM method, central bridges are equated with spokes, and the rotor pole with magnets and the rotor core are equated with an outer equivalent ring and an inner equivalent ring as in the conventional ERM methods [12]. The mechanical stresses at the central bridge $\sigma_{\text{cbm}}$ are determined as:

$$\sigma_{\text{cbm}} = \frac{Y}{A_{\text{sr}}} \tag{13}$$

where $A_{\text{sr}}$ is the radial cross-sectional area of the spokes, which is equal to the multiplication of the stack length and the thickness of the central bridge. The uniformly distributed tension on the inner ring Y is calculated as:

$$Y = X + \frac{q_s \omega^2}{2g} \left(R_2^2 - R_1^2\right) \tag{14}$$

where $R_1$ and $R_2$ are the inner and outer radii of the spokes. $q_s$ is the spokes average weight per unit.

The tension between the spokes and the outer ring X is recalculated due to a probable mistake in the formula given in [13] as:

$$X = \frac{\frac{4\pi q_0 R_0^2}{E A_0} - \frac{n R_v q_s \omega^2 (R_2^2 - R_1^2)}{4\pi E A_v g} - \frac{(R_2 - R_1) q_s \omega^2}{2 A_s g E} \cdot \left( R_2^2 - \frac{R_2^2 + R_2 R_1 + R_1^2}{3} \right)}{\frac{R_2 - R_1}{A_s E} + \lambda_0 + \frac{n R_v}{2\pi E A_v}} \tag{15}$$

where $q_0$ is the uniformly distributed inertial load, n is the number of spokes, E is the Young's modulus of electric steel, g is the gravitational acceleration, $\lambda_0$ is the flexibility coefficient of the outer ring, which express how the displacement along the centerline of the outer ring is influenced by the tension between the spokes and the outer ring, and $R_v$ is the centerline radius of the inner ring. $A_0$, $A_v$, $A_s$ represent the cross-sectional areas of the outer ring, the inner ring and the spokes. The equations for the defined symbols can be taken from [12].

### 2.2. Determination of Stress Concentration Factors

Chu et al. [13–15] proposed several methods to determine an accurate stress concentration factor (SCF) at the air gap bridges. The method proposed in [15] is considered in this study because it is applicable to a rotor geometry without considering a rotor pole number. The SCF at the air gap bridge $k_{\text{air gap bridge}}$ is determined as:

$$k_{\text{air gap bridge}} = 1.389 - 0.2374 \cdot \frac{d}{r_a} + 0.007181 \cdot \alpha + 0.03567 \cdot \left(\frac{d}{r_a}\right)^2$$
$$0.02148 \cdot \frac{d}{r_a} \cdot \alpha + 0.000745 \cdot \left(\frac{d}{r_a}\right)^3 - 0.001721 \cdot \left(\frac{d}{r_a}\right)^2 \cdot \alpha \tag{16}$$

where $r_a$ represents the notch radius at the air gap bridge as shown in Figure 5. The case of a stepped flat bar under tensile stress from [16] proposed by [12] is taken as an equivalent case to determine SCF at the central bridge $k_{\text{central bridge}}$ as:

$$\begin{aligned} k_{\text{central bridge}} = 1.97 - 0.384 \cdot \left(\tfrac{2r_c}{t+2r_c}\right) - 1.018 \cdot \left(\tfrac{2r_c}{t+2r_c}\right)^2 \\ +0.43 \cdot \left(\tfrac{2r_c}{t+2r_c}\right)^3 \end{aligned} \tag{17}$$

where $r_c$ is the notch radius on the central bridge as shown in Figure 5, and the constant numbers are presented in Reference [16] to determine the SCF.

### *2.3. Initial Conditions and Assumptions*

There are many factors such as thermal stress, rotor vibration, and unstable operation that affect the mechanical strength of a rotor. In this study, simplifications and initial conditions are assumed when evaluating the mechanical strength of IPMSMs in FEA. These assumptions can be considered feasible since the analytical approaches do not account for any of the simplified or neglected effects:

- Constant speed in steady state operation is assumed.
- Maximum deformation and stresses are mainly caused by centrifugal forces. The effect of electromagnetic forces between rotor and stator, and attraction forces between the permanent magnets and the rotor are considered negligible compared to centrifugal forces.
- Thermal effects are neglected.
- One pole in a two-dimensional model is used.
- The rotor core is assumed as an entity, and the lamination effects are considered negligible.
- Yield indicated by planar von Mises stress.
- The eccentricity of the rotor, the vibration, and the dynamic forces of the shaft are neglected.
- The analytical and numerical methods are based on the mono dimensional elastic theory. The inaccuracy of the methods proposed in this study increases with the mechanical stress above the yield point.

### *2.4. Investigated Machines*

Seven rotor geometries with different rotor topologies, including those of the e-machines of the Nissan Leaf vehicle (rotor 3) and the Toyota Prius III vehicle (rotor 4), are used to investigate the stability of the analytical methods [1]. The main parameters of investigated geometries are presented in Table 2. To verify the general applicability of the analytical methods, different rotor topologies such as flat shape, V-shape, double V-shape and delta shape, different sizes, and different speed ranges are considered. One pole of each rotor topology is shown in Figure 7.

**Table 2.** Geometries of the investigated rotors.

| Rotor Geometry | Geometry Definition/Unit | | | | |
|---|---|---|---|---|---|
| | Outer Diameter $R_o$/mm | Max. Speed/rpm | Air Gap Bridge Thickness d/mm | Central Bridge Thickness t/mm | Angle between Magnets θ/degree |
| Rotor 1 flat shape | 238 | 8000 | 1.26 | - | - |
| Rotor 2 flat shape | 206 | 11,200 | 1.8 | - | - |
| Rotor 3 delta shape | 130 | 10,400 | 0.7 | - | - |
| Rotor 4 V-shape | 160 | 13,500 | 1.94 | 1.8 | 146 |
| Rotor 5 V-shape | 206 | 11,200 | 2 | 2 | 170 |
| Rotor 6 V-shape | 146 | 18,100 | 2.3 | 3.4 | 137 |
| Rotor 7 double V-shape | 124 | 11,200 | 0.9 | 1.45 | 126 |

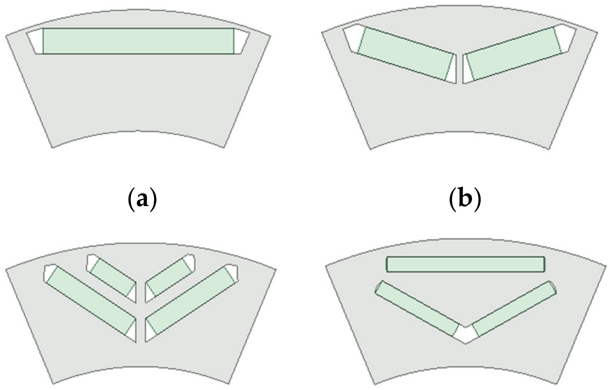

(**a**) (**b**)

(**c**) (**d**)

**Figure 7.** One pole view of the interior permanent magnet rotor geometries (**a**) flat shape, (**b**) V-shape, (**c**) double-V shape, (**d**) delta shape.

To determine the strength of the rotor geometries, FEA analyses were first performed to determine the location of the MMS and to visualize the stress distribution. Then, MMS at the air gap bridges for rotor 1, rotor 2 and rotor 3, and MMS at the central bridges for rotor 4, rotor 5, rotor 6 and rotor 7 were determined using the different analytical methods. To investigate the validity of these methods, the FEA results were taken as reference and the percentage difference between the FEA results and the analytical methods was determined.

The validity of the analytical methods was investigated over the speed range as well as through geometric design adjustments. To investigate the validity over the speed range, the speeds were changed from 1000 to 10,000 rpm. The design parameters shown in Figure 5 such as air gap bridge thickness (Figure 5d), magnet thickness (Figure 5h), notch radius on the air gap bridge $r_a$, notch radius on the central bridge $r_c$, and central bridge thickness were investigated by changing only the investigated parameter and keeping all other parameters constant. In addition, the entire rotor geometry was scaled to study the change in the stability of the analytical methods. The studied design parameters were changed in a reasonable range from half of the initial value to double the reference value.

The FEA analysis was performed using static structural analysis in ANSYS Workbench. Figure 8a shows the boundary conditions applied on a single rotor pole based on the assumptions and conditions given in reference papers [8,12,15,21]. A frictionless support was assumed on the symmetry axes to satisfy the symmetry condition. A cylindrical support on the inner surface of the rotor allowed the chosen nodes to move freely in radial direction, while preventing them to move on the tangential axis. Figure 8b shows the increased mesh density at the intersection points of air gap and central bridges where MMS can occur to achieve a converged solution. A rough contact between magnets and rotor core was assumed. Plane stress theory was assumed for the analysis of the rotor [11,12].

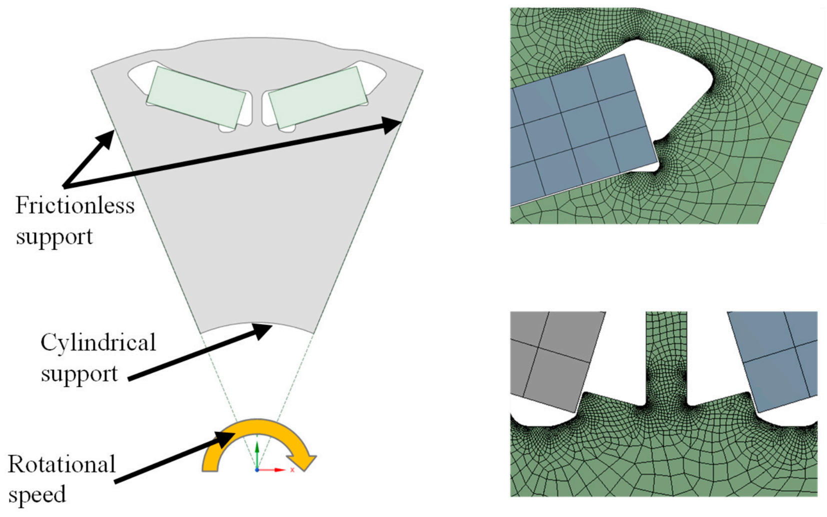


(a) (b)

**Figure 8.** (**a**) Boundary conditions for the FEA model, (**b**) mesh refinement at intersection points where maximum mechanical stress can occur.

## 3. Performance Review of the Methods and Results

For comparison, the results obtained with the different methods are presented in relative deviation (given as error in the following) to the FEA results. The FEA is taken as a reference, since experimental validation is out of the scope of this study, at this point. The relative percentage error between the analytical and FEA results is defined as:

$$\Delta\sigma = \frac{\sigma_{max,FEA} - \sigma_{max,analytical}}{\sigma_{max,FEA}} \quad (18)$$

where $\sigma_{max,FEA}$ is the maximal stress determined in FEA and $\sigma_{max,analytical}$ is the corresponding maximum stress of the respective method considered. The method that has the least error is considered to be the most suitable.

Since rotors 4 to 7 exhibit the maximum stress in the central bridge rather than in the air gap bridges, only BTM and CBM can be applied. Rotors 1, 2 and 3 do not have central bridges, the seven rotor geometries will therefore be split into variants with MMS in airgap bridges (see Table 3) and variants with MMS in central bridges, as shown in Table 4. Table 3 shows $\Delta\sigma$ at maximum speed for rotors 1 to 3, and from the table, it can be seen that errors for the ERM1 and ERM2 methods are close to each other, and they change about 70% for the selected geometries. This is relatively high compared to other methods, since a maximum spread of 33% is shown for the ERM 3 method, and a minimum of 15.5% for the CFM method is observable. Another drawback of ERM1 and ERM2 methods is shown by the high error for rotor 3. The reason is probably the different rotor topologies (rotor 3 is delta shaped). Here, the simplicity of ERM1 and ERM2, which only consider cross-sectional areas and do not consider the centroid radii, is shown to be a downside, as the stress for rotor 3 is overestimated by 55.6% and 56.2%, respectively. Considering that most traction machines usually have a V-shaped or delta-shaped rotor pole geometry, cf. (1), the ERM1 and ERM2 methods are not considered further in this study and are not further recommended to use for any delta-shaped geometry. Although the ERM3 and ERM4 methods take more information of the rotor geometry and material data into account, in this investigation, the resulting error to the FEA, ranging between 19.8% and 59.3%, is not satisfactory, especially since the analytical methods show an underestimation of the MMS.

**Table 3.** Evaluation of analytical methods to determine the maximum mechanical stress at the air gap bridges.

| Analytical Methods | Rotor Geometries | | |
|---|---|---|---|
| | Rotor 1 | Rotor 2 | Rotor 3 |
| ERM1 | −18.5% | 6.3% | 55.6% |
| ERM2 | −17.1% | 6.6% | 56.2% |
| ERM3 | 26.2% | 59.3% | 39.9% |
| ERM4 | 19.8% | 35.1% | 31.7% |
| ERM5 | −25.1% | −1.7% | −9.7% |
| CFM | −25.5% | −2.3% | −10.7% |
| BTM | 0% | −20% | −60% |
| FEA results | 348 MPa | 752 MPa | 350 MPa |

**Table 4.** Evaluation of the analytical methods to determine maximum mechanical stress at the central bridges.

| Analytical Methods | Rotor Geometries | | | |
|---|---|---|---|---|
| | Rotor 4 | Rotor 5 | Rotor 6 | Rotor 7 |
| BTM | 0% | 46.9% | −0.2% | −29% |
| CBM | −11% | 45.5% | −4.6% | −22% |
| FEA results | 341 MPa | 614 MPa | 487 MPa | 121 MPa |

The ERM5 and CFM methods achieve an error of less than 2.5%, with ERM5 showing the lowest error compared to the FEA results. It ranges from 1.7% to 25.1% and gives overestimations and thus a worst-case estimation for the rotor geometries studied. The ERM5 method is chosen for further stability investigations for the MMS at the air gap bridges, since it shows the least error, considering all investigated rotor geometries, and uses a simple equivalent model. This gives the benefit that possible future error and discrepancies can be corrected more easily.

The BTM method was initially applied to the geometries of rotor 1 and rotor 4 for the air gap bridges and the central bridges, respectively. As mentioned earlier, the BTM method requires an initial fitting with a first rotor geometry. This was conducted for rotor 1 and rotor 4. After fitting, naturally, the error for the fitted rotors is 0. For the other rotors, such a fitting was not performed. Considering a comparative study with multiple rotors, or a development process with significant rotor geometry changes, a repeated fitting process with FEA is not very realistic. Table 3 shows the high error for BTM for stress in the airgap bridge of up to −60%. Table 4 also shows a high deviation for BTM. However, for stresses in the central bridge, the error is in general lower and closer to the error of the CBM method. The unstable behavior after any significant change in the rotor geometries, despite the initial fitting of the BTM method for stress in the airgap bridge, leads to the conclusion that the BTM method is not recommend for MMS estimation in the airgap bridge and will be not considered in further stability investigations.

The CBM method is selected as the most suitable method for determining the MMS at the central bridges, especially because the method does not require an initial fitting compared to the BTM method. The MMS is overestimated for rotors 4, 6 and 7. The highest deviation is rotor 7 with −29%. Rotor 7 shows the highest deviation for BTM and CBM (excluding rotor 5), which is likely due to its double V-shaped geometry. As can be seen in Table 4, the CBM as well as BTM method show a relatively high error for rotor 5. The reason for that is explained in [12]. It is concluded that when the angle between two magnets is close to 180 degrees, the method does not provide an MMS estimate that is close to the actual expected values due to the uniform distribution of mass density at the rotor pole. Therefore, Rotor 5 is not considered in further investigations.

In order to investigate the behavior of the method over the entire speed range of the machines, Figures 9 and 10 show the MMS at the air gap bridge and the central bridge, respectively. The determined MMS in FEA and the selected analytical methods in the particular speed range are shown for rotors 1 to 3 and for rotors 4, 6 and 7. Additionally the error of each method is shown. It can be observed that for chosen methods, ERM 5 and CBM methods, the resulting error is stable over the whole speed range and is close to the given numeric value in Table 3.

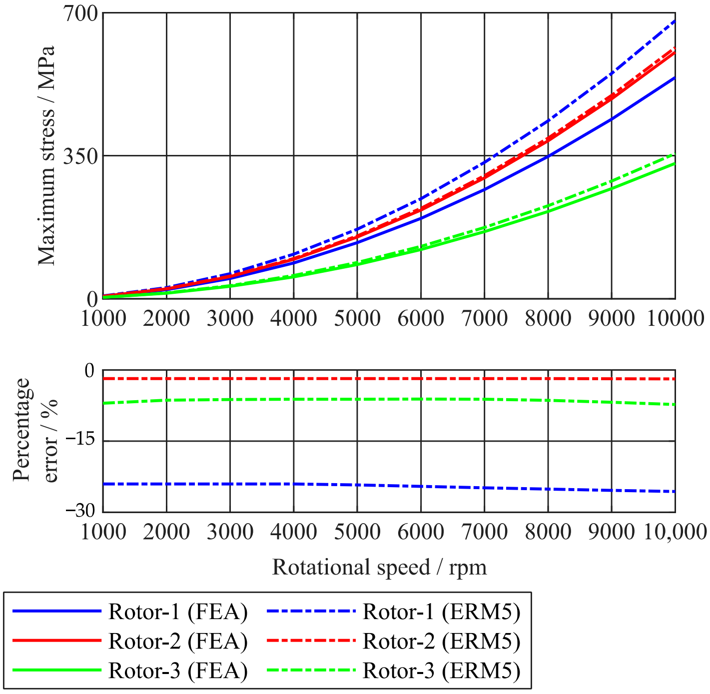


**Figure 9.** Stability analysis of the ERM5 method vs. rotor speed for different rotor geometries.

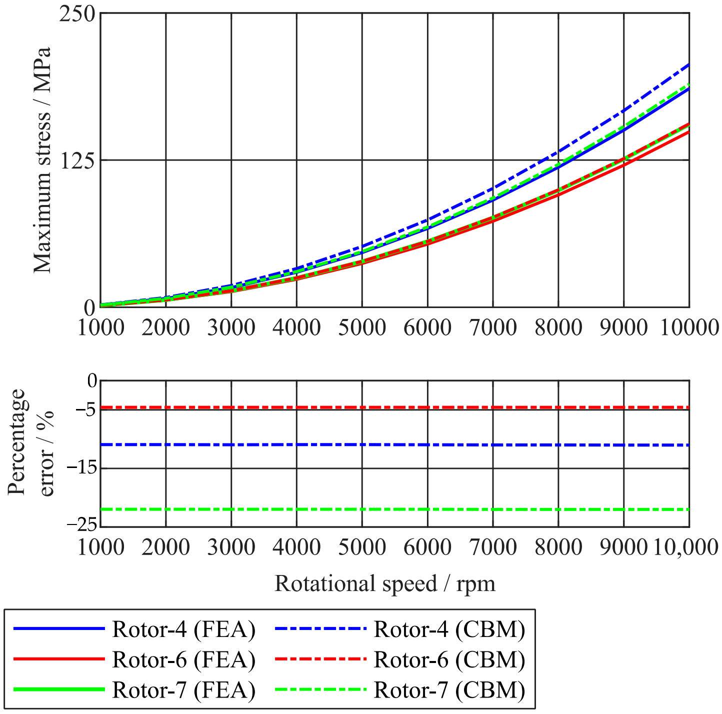


**Figure 10.** Stability analysis of the CBM method vs. rotor speed for different rotor geometries.

For development processes, the MMS could be investigated for geometry variations in a given rotor design. For this approach, a stable behavior of the method is required for specific geometry changes. The stability of selected rotor geometries under geometric design variations is presented in Figures 11 and 12. In this study, universal rotor geometry parameters are chosen, namely airgap bridge thickness, magnet thickness, notch radius and a general geometry scaling. The range of the parameters was chosen arbitrarily from 50% to 200% of the original value. This is a rather wide variation range especially for airgap and central bridge thickness, and the upper and lower limits might not be a typical rotor geometry, which could also affect the results of the analytical approaches and FEA simulations. The stability of the notch radius is only investigated for rotor 1 and rotor 4 geometries. Since the SCF is only dependent on the notch radius, but not dependent on the analytical methods, it is expected to have the same stability for different geometries. For the ERM5 method, magnet and core area will definitely be considered. However, the airgap bridge thickness will affect the actual stress in the rotor. This does not seem to be captured by the ERM5 method, as can be seen in Figure 11, where the error for an increased airgap bridge is increased for all rotor geometries (maximal by 25% and around 12% for rotor 2 and rotor 3). The geometry scaling seems to have the least effect on the resulting error; here, a slightly higher effect on the ERM5 is visible (below 10%) compared to the CBM (below 5%). In terms of overall error, geometry scaling can be performed accurately with ERM and CBM. For ERM5, a reduced magnet thickness compared to the original geometry shows a significant underestimation of the MMS, especially for rotor 3 (delta-shaped rotor). This again indicates that the more complex rotor geometry must be treated with caution using the simple ERM model. The variation of the central bridge thickness with regard to CBM is comparable to the variation of the airgap bridge thickness with ERM5. Examination of the CBM error with variation of the central bridge thickness shows the highest change in error (around 40% for rotor 6 and rotor 7), while variations in magnet thickness and geometry scaling are well below 10%.

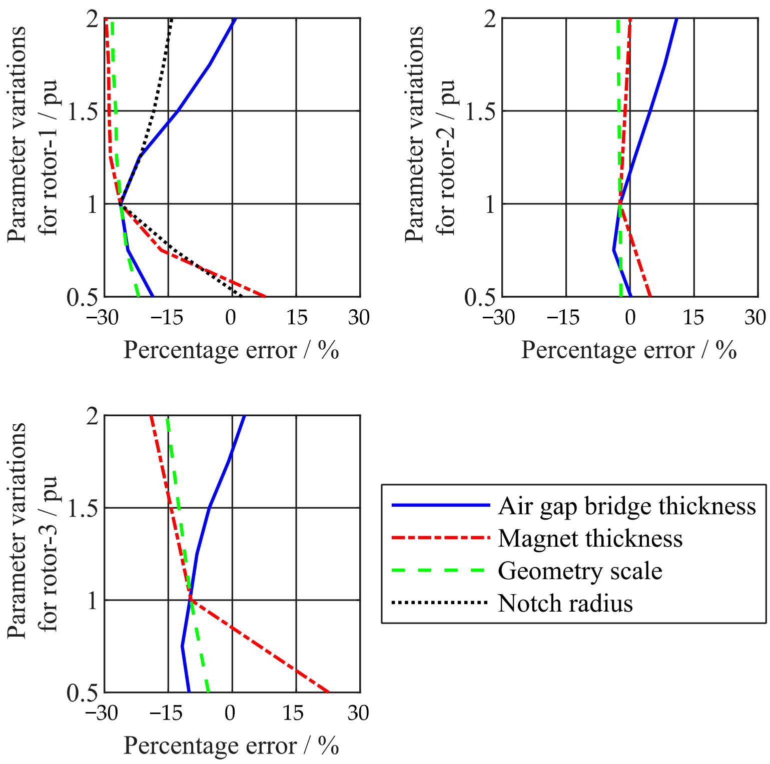


**Figure 11.** Stability analysis of the ERM5 method for parameter variations of various rotor geometries.

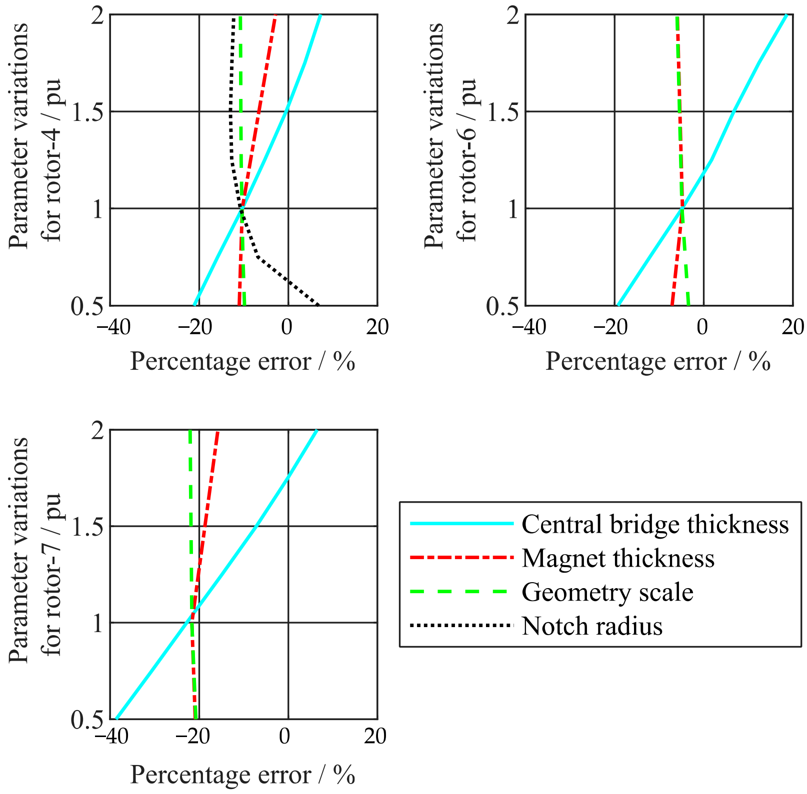


**Figure 12.** Stability analysis of the CBM method for parameter variations of various rotor geometries.

## 4. Conclusions

The maximum speed of electrical machines used as traction drives is increasing due to the requirements for higher power density. In order to ensure the mechanical stability of the electric machines, simulations or estimations must be carried out in the design process, in particular, for the mechanical loads due to the centrifugal forces acting on the rotor. Appropriate analytical methods have been developed to achieve acceptable values for computation times and manpower requirements. Published approaches were used for electrical machines available on the market, and the resulting accuracy (compared to finite element analyses as reference) was verified. In addition, the stability of these methods was investigated with variations in operating speed and rotor dimensions. The methods that show the highest accuracy for the maximum mechanical stress at airgap bridges are equivalent ring method 5, and for central bridges the central bridge method. These two methods show errors of less than 25.1 and 22%, respectively, for the selected rotor geometries. Parameters such as magnet thickness, air gap bridge thickness, central bridge thickness, notch radius and geometry scale were studied for the methods with the highest accuracy to verify the stability of these methods.

For future work, especially for early development stages, the equivalent ring method 5 can be used for fast evaluation process, since it was found that the estimates are feasible even if the geometry is significantly changed. Additionally, stress concentration factor for the central bridge will be identified for a more general use. For an improved and more holistic approach, a merged method combining equivalent ring method 5 and the central bridge method will be developed and benchmarked with even more recent traction motor geometries.

**Author Contributions:** Conceptualization, C.M.; methodology, M.E.A.; software, M.E.A.; validation C.M., M.E.A. and A.K.; formal analysis, M.E.A. and C.M.; investigation, M.E.A.; resources, A.K.; data curation, M.E.A. and C.M.; writing—original draft preparation, M.E.A.; writing—review and editing, C.M., A.K. and J.A.; visualization, M.E.A.; supervision, C.M.; project administration, J.A. and C.M. All authors have read and agreed to the published version of the manuscript.

**Funding:** This research received no external funding.

**Data Availability Statement:** The data that support the findings of this study are from FEV Europe GmbH. Restrictions apply to the availability of these data, which were used under license for this study. Data are available upon reasonable request from the authors with the permission of FEV Europe GmbH.

**Conflicts of Interest:** The authors declare no conflict of interest.

## List of Symbols

| | |
|---|---|
| $\rho_{Fe}$, $\rho_m$ | Mass density of electric steel and magnet material |
| $\rho_{eq,erm}$ | Density of equivalent ring |
| $A_{Fe}$, $A_m$, $A_{eq}$ | Cross-sectional area of rotor pole, permanent magnets and equivalent ring |
| $\sigma_{eq,erm}$, $\sigma_{eq,max}$ | Tangential and maximum stresses inside equivalent ring |
| $R_{eqo}$, $R_{eqi}$ | Outer and inner radiuses of equivalent ring |
| $\omega$ | Rotational speed |
| $k_{air\ gap\ bridge}$, $k_{central\ bridge}$ | Stress concentration factor at the air gap and central bridges |
| $G_{Fe}$, $G_m$, $G_c$ | Center of gravity of rotor pole, magnets and rotor pole with magnets |
| $R_{Fe}$, $R_m$, $R_0$ | Centroid radius of rotor pole, magnets and equivalent ring |
| $\theta$ | Angle between two magnets of a single pole |
| $\nu$ | Poisson's ratio |
| $R_c$ | Centroid radius of rotor pole with magnets |
| d, t | Air gap and central bridge thicknesses |
| $\alpha$ | Half pole arc |
| $c_1$, $c_2$, $c_3$ | Constant coefficients for the relationship between centrifugal force, normal force and bending moment |
| $m_{total}$ | Total mass of rotor pole with magnets |
| $l_{stack}$ | Stack length |
| $A_{sr}$ | Radial cross-sectional area of spokes |
| Y | Uniformly distributed tension on the inner ring |
| X | Tension between spokes and outer ring |
| $R_1$, $R_2$ | Inner and outer radii of spokes |
| $q_s$ | Spokes average weight per unit |
| $q_0$ | Uniformly distributed inertial load gravitational acceleration |
| n | Number of spokes |
| E | Young's modulus |
| g | Gravitational acceleration |
| $\lambda_0$ | Flexibility coefficient of outer ring |
| $R_v$ | Centerline radius of inner ring |
| $A_0$, $A_v$, $A_s$ | Cross-sectional areas of outer ring, inner ring and spokes |
| $r_a$, $r_c$ | Notch radius on the air gap and central bridges |

## References

1. Krings, A.; Monissen, C. Review and Trends in Electric Traction Motors for Battery Electric and Hybrid Vehicles. In Proceedings of the 2020 International Conference on Electrical Machines (ICEM), Gothenburg, Sweden, 23–26 August 2020; pp. 1807–1813.
2. Burress, T. Electrical Performance, Reliability Analysis, and Characterization. Available online: https://www.energy.gov/sites/prod/files/2017/06/f34/edt087_burress_2017_o.pdf (accessed on 10 November 2020).
3. CORPORATION TM. The Evolution of the Prius [Internet]. Toyota Motor Corporation Official Global Website. Available online: http://global.toyota/en/detail/17852348 (accessed on 10 November 2022).
4. Lee, K.J.; Kim, K.C.; Lee, J. Bridge optimization of interior permanent magnet motor for hybrid electric vehicle. In Proceedings of the 2003 IEEE International Magnetics Conference (INTERMAG), Boston, MA, USA, 30 March 2003–3 April 2003; p. GQ-07.
5. Lovelace, E.C.; Jahns, T.M.; Keim, T.A.; Lang, J.H. Mechanical design considerations for conventionally laminated, high-speed, interior PM synchronous machine rotors. *IEEE Trans. Ind. Appl.* **2004**, *40*, 806–812. [CrossRef]
6. Powercore® for High Frequencies and e-Mobility [Internet]. Thyssenkrupp. Available online: https://www.thyssenkrupp-steel.com/en/products/electrical-steel/electrical-steel-non-grain-oriented/powercore-for-high-frequencies-and-e-mobility/powercore-a-3.html (accessed on 23 November 2022).

7. High-Strength Electrical Steel Strip: HS Grades for High Mechanical Stress [Internet]. Waelzholz. Available online: https://www.waelzholz.com/en/steel-materials/electrical-steel-strip/hs-grades.html (accessed on 19 September 2022).
8. Han, Z.; Yang, H.; Chen, Y. Investigation of the rotor mechanical stresses of various interior permanent magnet motors. In Proceedings of the 2009 International Conference on Electrical Machines and Systems, Tokyo, Japan, 15–18 November 2009; pp. 1–6.
9. Barcaro, M.; Meneghetti, G.; Bianchi, N. Structural Analysis of the Interior PM Rotor Considering Both Static and Fatigue Loading. *IEEE Trans. Ind. Appl.* **2014**, *50*, 253–260. [CrossRef]
10. Rao, J.; Qu, R.; Ma, J.; Xu, W. Investigate the influence of magnetic bridge design on mechanical strength and electromagnetic characteristics in high speed IPM machines. In Proceedings of the 2014 17th International Conference on Electrical Machines and Systems (ICEMS), Hangzhou, China, 22–25 October 2014; pp. 22–27.
11. Cha, K.-S.; Kim, D.-M.; Park, M.-R.; Yoon, M.-H.; Hong, J.-P. Multipolar High-Speed IPMSM Design for EV Traction Considering Mechanical Stress. In Proceedings of the 2016 IEEE 84th Vehicular Technology Conference (VTC-Fall), Montreal, QC, Canada, 18–21 September 2016; pp. 1–6.
12. Iacchetti, M.F.; Popescu, M.; Goss, J. Combined Analytic-Linear-FE Approach for Fast Stress Analysis of High-Speed Interior PM Rotors. In Proceedings of the 2019 IEEE International Electric Machines Drives Conference (IEMDC), San Diego, CA, USA, 12–15 May 2019; pp. 280–287.
13. Chai, F.; Li, Y.; Liang, P.; Pei, Y. Calculation of the Maximum Mechanical Stress on the Rotor of Interior Permanent-Magnet Synchronous Motors. *IEEE Trans. Ind. Electron.* **2016**, *63*, 3420–3432. [CrossRef]
14. Chu, G.; Dutta, R.; Rahman, M.F.; Lovatt, H.; Sarlioglu, B. Analytical Calculation of Maximum Mechanical Stress on the Rotor of Interior Permanent-Magnet Synchronous Machines. *IEEE Trans. Ind. Appl.* **2020**, *56*, 1321–1331. [CrossRef]
15. Chu, G.; Dutta, R.; Lovatt, H.; Sarlioglu, B.; Rahman, M.F. Analytical Calculation of Maximum Mechanical Stress on the Rotor of the Interior Permanent-Magnet Synchronous Machine. In Proceedings of the 2018 IEEE Energy Conversion Congress and Exposition (ECCE), Portland, OR, USA, 23–27 September 2018; pp. 255–261. [CrossRef]
16. Pilkey, W.D.; Pilkey, D.F.; Bi, Z. *Peterson's Stress Concentration Factors*; John Wiley & Sons: Hoboken, NJ, USA, 2020; 640p.
17. Bremner, R.D. Bridge stresses and design in IPM machines. In Proceedings of the IEEE EUROCON 2009, St. Petersburg, Russia, 18–23 May 2009; pp. 655–662.
18. Kleilat, I.; Langue, L.N.; Friedrich, G.; Vivier, S.; Kadri Benkara, K.E. Comparison between Assisted and Dual Phase synchronous reluctance machines for high speed applications. In Proceedings of the 2018 IEEE Energy Conversion Congress and Exposition (ECCE), Portland, OR, USA, 23–27 September 2018; pp. 1648–1655.
19. Schätzer, C. *Ein Verfahren zur Optimierung bei Elektrischen Maschinen mit Hilfe der Numerischen Feldberechnung*; Shaker: Aachen, Germany, 2002; 167p.
20. Binder, A.; Schneider, T.; Klohr, M. Fixation of buried and surface-mounted magnets in high-speed permanent-magnet synchronous machines. *IEEE Trans. Ind. Appl.* **2006**, *42*, 1031–1037. [CrossRef]
21. Yi, L.; Yulong, P.; Peixin, L.; Feng, C. Analysis of the rotor mechanical strength of interior permanent magnet synchronous in-wheel motor with high speed and large torque. In Proceedings of the 2014 IEEE Conference and Expo Transportation Electrification Asia-Pacific (ITEC Asia-Pacific), Beijing, China, 31 August–3 September 2014; pp. 1–5.
22. Kleilat, I.; Kadri Benkara, K.E.; Friedrich, G.; Vivier, S.; Moubayed, N.; Dib, R. Comparison of two Analytical Methods for Calculating the Maximum Mechanical Stress in the Rotor of High Speed Assisted Synchronous Reluctance Machines. In Proceedings of the 2019 IEEE Energy Conversion Congress and Exposition (ECCE), Baltimore, MD, USA, 29 September–3 October 2019; pp. 1669–1674.
23. Young, W.C.; Budynas, R.G.; Sadegh, A.M. *Roark's Formulas for Stress and Strain*, 8th ed.; McGraw Hill Professional: New York, NY, USA, 2011; 1073p.